Simulating charge transport in tris(8-hydroxyquinoline) aluminium (Alq_3)

J. J. Kwiatkowski,[a] J. Nelson,[a] H. Li,[b] J. L. Bredas,[b] W. Wenzel[c] and C. Lennartz[d]

We present a model of charge transport in organic solids which explicitly considers the packing and electronic structure of individual molecules. We simulate the time of flight mobility measurement in crystalline and disordered films of tris(8 hydroxyquinoline) aluminium (Alq_3). The morphology of disordered Alq_3 is modelled on a molecular scale, and density functional theory is used to determine the electronic couplings between molecules. Without any fitting parameters we predict electron mobilities in the crystalline and disordered phases of ~ 1 and $\sim 10^{-4}\,cm^2\,V^{-1}\,s^{-1}$, respectively. In good agreement with experiment we find that electron mobilities are two orders of magnitude greater than those of holes. We explain this difference in terms of the spatial extent of the frontier orbitals. Our results suggest that charge transport in disordered Alq_3 is dominated by a few highly conducting pathways.

1. Introduction

Organic electronic materials offer the potential for optoelec tronic devices that are cheap, lightweight, flexible and which could be employed for a wide range of applications including solar cells and large area displays. However, the performance of all such devices depends critically on the rate of charge transport in organic materials.[1,2] Encouragingly, organic tran sistors have been made with charge mobilities that are com parable to those of amorphous silicon.[3] However, the highest charge mobilities are obtained in single organic crystals[4] which are not practical for large scale applications. On the other hand cheaper fabrication techniques such as vacuum sublima tion or solution processing produce disordered films whose mobilities are orders of magnitude lower than those of crystals.[5] Therefore, the success of organic electronics depends largely on the ability to systematically improve charge mobilities in disordered organic materials.

Despite the huge interest in the subject, the factors that limit charge mobility in disordered organic films remain poorly understood. Whereas the theory of charge transfer between single molecules has been described in detail[6,7] there is little work that rigorously considers charge transport on a larger scale. In part this is because charge mobility is sensitive to a wide range of factors including the way molecules pack to make a film.[8,9] Moreover, because of the computational cost of scaling from individual molecules to solid films, previous simulations have generally relied upon simplified models with empirical fitting parameters, such as the Gaussian disorder model.[10] Though able to fit experimental data reasonably well[11] these models remain unable to predict the charge mobility from molecular properties; as such they are of limited use for systematically designing more conductive organic films. Recent papers have presented models of charge transport that consider the effect of molecular packing in one dimensional liquid crystals[12] and highly stylised three dimensional morpho logies.[13] We extend on these results by considering charge transport in a three dimensional disordered solid. We present simulations of charge transport in crystalline and disordered tris(8 hydroxyquinoline) aluminium (Alq_3). Alq_3 is commonly used in organic light emitting diodes and has particularly interesting charge transport characteristics because of its large electron mobility which, unusually for organic semiconductors, is higher than its hole mobility.[14] We extend upon previous theoretical comparisons of hole and electron transport in Alq_3 which have been limited to the crystalline phase.[15,16]

We construct realistic molecular models of extended three dimensional samples of disordered Alq_3 by a process that emulates molecular beam epitaxy. On the basis of this struc tural model we perform electronic structure calculations using density functional theory (DFT); although this method is computationally expensive and limits the size of our simula tions it has been shown that accurate results demand this treatment.[17]

2. Methodology

2.1 Overview

We generate disordered morphologies with a Monte Carlo method that simulates physical deposition of molecular films; the full details are described in section 2. We take our samples to be free of all impurities and neglect the thermal vibrations of molecules.[18] We consider that charges move through Alq_3 by hopping between neighbouring molecules with a rate k_{if} described by semi classical Marcus theory[19]

$$k_{if} = \frac{|J_{if}|^2}{\hbar}\sqrt{\frac{\pi}{\lambda k_B T}}\exp\left(\frac{(\Delta G_{if}+\lambda)^2}{4\lambda k_B T}\right) \qquad (1)$$

[a] *Department of Physics, Imperial College, London, UK SW7 2AZ. E mail: jk905@ic.ac.uk*
[b] *School of Chemistry and Biochemistry, Georgia Institute of Technology, Atlanta, USA*
[c] *Institute für Nanotechnologie, Universität Karlsruhe, Karlsruhe, Germany*
[d] *Computational Chemistry, BASF AG, Ludwigshafen, Germany*

Here λ is the reorganisation energy, J_{if} is the electronic coupling between the initial and final state and ΔG_{if} is the change in free energy. Our use of eqn (1) is justified by the fact that λ is large compared to J_{if} as discussed in section 3. We calculate J_{if}, ΔG_{if} and λ for each pair of neighbouring molecules using density functional theory. The k_{if} are then used to calculate charge mobilities in kinetic Monte Carlo simulations of the time of flight (ToF) experiment:[11] charges are generated in a thin layer on one side of the film and then drift under an applied electric field until they are collected on the opposite side. As the charges drift across the film they induce a photocurrent in an external circuit. We calculate the mobility as

$$\mu = \frac{\langle v \rangle}{F} \tag{2}$$

where $\langle v \rangle$ is the average velocity of charges in the direction of the field averaged over many simulations and F is the electric field.

2.2 Film deposition

There are two low temperature solvent free crystalline phases of Alq_3, α and β;[20] in keeping with previous theoretical studies[15,16] we consider the latter. Both the β phase and amorphous films are constituted from the meridional isomer of Alq_3.[20,21]

The disordered phase was simulated by depositing molecules individually using an adapted basis hopping method[22–24] on top of a surface modelled as an impenetrable plane. These simulations make a deposition of many thousand molecules feasible because they focus the numerical effort on the crucial phase of the deposition process where the molecule finds its position on the surface. The basin hopping approach may be best understood as a coarse grained Monte Carlo scheme. In most Monte Carlo simulations an individual step consists of a microscopic change in the conformation of one or a few particles of the system. On a very rugged potential energy surface, such as those induced here by the roughness of the partially deposited film, such simulations are often trapped for long times in long lived metastable conformations. Such entrapment would result in films with a much lower density than those observed experimentally, because the time scale which can be realistically sampled with present day atomistic simulation methods is many orders of magnitude smaller than that of the experiment.

In principle, however, the move construction in Monte Carlo schemes is not limited to small individual steps, as long as the simulation remains ergodic. Instead, one may move a particle randomly and then minimise its energy before considering acceptance. Because of the intermediate minimisation step only low energy conformations are compared with one another, which greatly enhances the acceptance probability of the considered conformational change. Depending on the minimisation method used, the proposed steps (called basin hopping cycles) may be large scale nontrivial conformational changes. Obviously the construction of such moves is much more expensive than standard conformational Monte Carlo moves. However, since the escape time from deep energy minima with small scale moves may be exponentially long (depending on the barrier to be overcome), this numerical investment into the move construction may lead to an overall speedup of the simulation, which is no longer trapped as easily in metastable conformations. In our experience, gradient based minimisation methods[23,24] are not always an ideal choice to find a very good proposal for the next large scale move, because the local gradient on rugged energy surfaces carries little information about the position of the next low lying metastable conformation. Instead we used simulated annealing[25] as a move generator for the basin hopping cycles. In this method, many small scale moves are performed starting at a high temperature, which permits barrier crossing. Then the temperature is gradually decreased to some final temperature. In the limit of adiabatic cooling (which is obviously not reached in practice) this method equilibrates the system to its thermodynamic equilibrium ensemble at the final temperature. If the final temperature is zero, this corresponds to the global optimum of the energy surface thus simulated annealing can be viewed as a thermodynamically motivated minimisation method. For materials simulations that aim to describe a system at some finite temperature, this approach has the charm that the final temperature of the simulated annealing cycle may be chosen as the ambient temperature, thus generating conformations from the appropriate thermodynamic ensemble.

Each molecule was initially placed randomly above the surface and was subjected to inter molecular forces (we used the all atom Dreiding potential[26]) of the other molecules and to a weak linear potential towards the surface. Periodic boundary conditions were applied parallel to the surface. This guiding potential was necessary to reduce the time of random diffusion, or even escape away from the surface, when the particle was far from the surface and the intermolecular forces small. The guiding potential was switched off when the molecule approached the surface. For each molecule we performed 10 basin hopping cycles, each of which consisted of a simulated annealing run[25] with 5000 steps starting from the last accepted basin hopping cycle. The simulated annealing simulations used a starting temperature of 500 K and a geometric cooling schedule to a final temperature of 5 K. The individual steps in the simulated annealing simulation consisted of equal parts of rigid body displacements, drawn from a Gaussian distribution with a standard deviation of 1 nm, and rigid body rotations around a random axis with an angle drawn from a Gaussian distribution with a standard deviation of 2π. Conformations at the end of the annealing cycle were accepted only when their energy was lower than that of the previous conformation. The progress of the simulation for the deposition of ten molecules (starting with molecule 120) is shown in Fig. 1. The spike in energy at the beginning of each deposition corresponds to the initial placement. Each basin hopping cycle starts with a high temperature, permitting the particle to attain a comparatively high energy which permits barrier crossing, but the energy falls as the system is cooled. As a result, the energies at the end of the basin hopping cycle are comparable to those at the beginning, generating an appreciable acceptance rate in the simulation. As a result the particle explores the surface on the nanometer scale (central panel) even though the surface is very rough (bottom panel). As a result, a dense morphology is generated using an

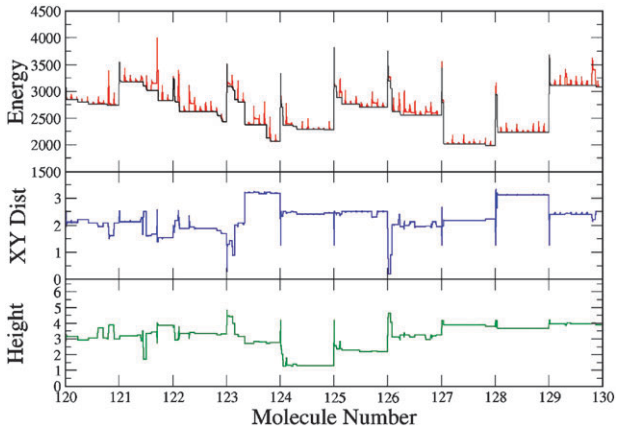

Fig. 1 Illustration of the deposition method for ten molecules starting at molecule number 120. One major tick mark on the horizontal axis summarises 10 basin hopping simulations as described in the text. The top panel shows the energy (arbitrary units): the red curve shows the instantaneous energy during a simulated annealing simulation (basin hopping cycle), the black curve the energy of the accepted conformation in the basin hopping simulations. The centre panel shows the displacement of the particle in XY direction relative to its starting position while the bottom panel shows the height of the particle (both in nm).

atomistic, material specific potential, which may not be attainable by kinetic methods, such as molecular dynamics. The deposition of an individual particle takes less than a minute on a standard PC, as a result films with many thousand molecules can be deposited in a reasonable time.

2.3 Quantum chemical calculations

We calculate intermolecular hopping rates between all neighbouring molecules. In the crystalline phase neighbours are defined as two molecules with an electronic coupling J_{if} greater than 0.5 μeV whereas in the disordered phase neighbours are taken as molecules with centres of mass that are within 13 Å of each other.

Most INDO based calculations which use the "energy splitting in dimer" method[17] often over estimate electronic couplings and also ignore the orthogonalisation of the basis set; we address these issues by using DFT to calculate J_{if}. Within the tight binding approximation[27] electronic couplings are defined as the off diagonal matrix elements of the two dimensional tight binding Hamiltonian operator H of the pair of molecules which satisfies the eigenvalue equation

$$HC \quad SCE \tag{3}$$

where C is the eigenvector matrix with the basis set formed from the molecular orbitals of the two individual molecules, S is the overlap matrix and E is the diagonal eigenvalue matrix. The electronic structures are calculated at the DFT level with the generalised gradient approximation of PW91[28] realised within the ADF package.[29] Experimental molecular structures are used in the crystalline phase but for the amorphous system the molecular structures are obtained from the morphology simulations. In both systems the electronic structure of the individual molecules are first calculated to generate the molecular orbitals which will be used as the basis set for the pair; the frontier orbitals are shown in Fig. 8. Usually, when describing the pair's electronic states, such as the lowest unoccupied molecular orbital (LUMO) [or highest occupied molecular orbital (HOMO)], only the two LUMOs (or HOMOs) of the individual molecules are needed as the expansion basis set. Under the tight binding approximation, the electronic coupling can be written as

$$J_{if} \quad \langle \phi_i | H | \phi_f \rangle \tag{4}$$

where $|\phi_i\rangle$ is the HOMO (or LUMO) of the molecule which is occupied in the initial state and $|\phi_f\rangle$ is the HOMO (or LUMO) of the molecule which is occupied in the final state.

However, for some pairs of neighbours the LUMO states are described by the combinations of the LUMO and LUMO + 1 states of the individual molecules, instead of only the LUMO states as described above. For instance, the contribution from the LUMO + 1 state of the monomer can be larger than 20% with the LUMO state contribution concomitantly smaller than 80%. Although the energy difference between the LUMO and LUMO + 1 states of individual molecules is larger than 0.2 eV, the large contribution of the LUMO + 1 to the LUMO of the pair should not be overlooked in the electronic coupling calculations. This problem has been solved by applying the "mixed state" definition of the electronic coupling. In this definition, the LUMO and LUMO + 1 states of individual molecules are combined as a "mixed state" and the "four state" problem is therefore converted to a "two state" problem which can be solved within the two state tight binding approximation. The detailed computational process can be found in ref. 27 and will not be discussed in this work. We have applied the "mixed state" definition to the electronic coupling calculations; the transfer integrals calculated for the crystalline structure are given in Table 1.

We neglect entropic effects and approximate the free energy ΔG_{if} by

$$\Delta G_{if} \quad \Delta\varepsilon_{if} + q(\mathbf{r}_{if})\cdot\mathbf{F} \tag{5}$$

where $\mathbf{r}_{if}$ is the vector between molecule i which is occupied in the initial state and molecule f which is occupied in the final state; q is $\pm e$ depending on whether we are considering holes or electrons. $\Delta\varepsilon_{if}$ is the difference between the energies of the initial and final states. In the β crystal phase of Alq_3 the two molecules in the unit cell are related by inversion symmetry so $\Delta\varepsilon_{if}$ 0 and the electric field is the sole contributor to ΔG_{if}. In the amorphous phase, the position of each molecule is unique and consequently the site energies of all molecules are different. Because of the computational expense of calculating $\Delta\varepsilon_{if}$ for a large number of molecules we are limited to taking $\Delta\varepsilon_{if}$ as the difference between eigenvalues in eqn (3). This is a very rough approximation because we only consider the frontier orbitals of the two molecules involved in the charge transfer reaction and neglect all surrounding molecules. However, we find that the distribution of $\Delta\varepsilon_{if}$ is roughly a Gaussian with a standard deviation of 0.2 eV which is consistent with the values expected for the energetic disorder in the Gaussian disorder model.[10]

We separate the reorganisation energy λ into an inner and outer energy, λ_i and λ_o, respectively.[6] We take the inner reorganisation energy λ_i for the meridional isomer of Alq_3 as

Table 1 The twelve different neighbouring pairs in the β phase of Alq_3 for which $J_{if} > 0.5$ μeV. Both molecules in the unit cell possess identical lists of neighbours except that the displacements are inverted

Pair	Cell[a]	$\mathscr{I}$[b]	J_{if}/meV
1	(0, 1, 1)	✓	92.59
2	(1, 1, 1)	✓	31.12
3	(0, 1, 0)	✓	2.439
4	(0, 0, 1)	✓	6.683
5	(1, 1, 0)	✓	1.703
6, 7	(±1, 0, 0)	×	1.419
8	(1, 0, 1)	✓	9.094×10^{1}
9, 10	(0, ±1, 0)	×	7.027×10^{1}
11	(1, 0, 0)	✓	3.041×10^{2}
12	(0, 0, 0)	×	5.04×10^{4}

[a] The cell in which the neighbouring molecule is located. [b] Centre of inversion between molecules.

0.276 and 0.242 eV for electrons and holes, respectively, according to ref. 15. The external reorganisation energy is more difficult to quantify because it originates from the polarisation of the surrounding medium and includes the polarisation caused by electron phonon coupling as well as pure electronic polarization.[7] For crystalline anthracene, the contribution from the coupling of the electron and the acoustic phonon has been estimated to be about 0.04 eV.[30] In the current work, we neglect λ_o in the first instance and consider it only in order to observe the effect it has on the value of the charge mobility.

2.4 Kinetic Monte Carlo simulations

We simulate the time of flight experiment using a kinetic Monte Carlo approach similar to that in ref. 31 except that we make no approximations about the film morphology and calculate k_{if} explicitly for all pairs. We simulate charge transport through crystals of Alq_3 that measure $1 \times 0.03 \times 0.03$ μm where the long axis is aligned with the electric field and periodic boundary conditions are applied in the other dimensions. Simulations on amorphous Alq_3 are limited by the computational cost of the DFT calculations; we are therefore restricted to much smaller samples. The largest sample we are able to consider contains 1137 molecules and measures $10 \times 10 \times 10$ nm. We model charge transport parallel to the surface on which the sample was grown and we average our results over electric fields applied in different directions.

Charges are generated randomly in the bottom 5% of the sample and collected in the top 5%. In the large crystalline sample we consider 200 charges; in the disordered sample we introduce fewer than 5 charges. We find that up to a density of 0.01 charges per molecule ($\sim 10^{-19}$ cm^{-3}) the mobilities are only very weakly dependent on the number of photogenerated charges.

3. Results

3.1 Crystalline Alq_3

Table 1 shows the values of J_{if} that exceed 0.5 μeV for pairs of molecules in the β phase of Alq_3. Since λ_i is three times greater than the largest J_{if} we can consider that charge transfer is in the non adiabatic regime[18] (even if we take λ_o 0) and we therefore calculate the charge hopping rate with eqn (1).

A typical photocurrent transient for crystalline Alq_3 is shown in Fig. 2; the transient is non dispersive as expected from a highly ordered material. We simulated charge transport perpendicular to each face of the unit cell; Fig. 3 shows that depending on the direction of the field the mobility can vary by over an order of magnitude. Although we are not aware of any published mobility measurements for crystalline Alq_3 our mobilities are of the same magnitude as those measured in other organic crystals[32] and a similar anisotropic mobility has been observed in single crystals of pentacene.[33] For crystalline bathocuproine and bathophenanthroline, whose charge transfer is also in the non adiabatic regime, we predict mobilities that are similar to those of Alq_3. Although it has been shown that charge transport in crystalline pentacene is *not* non adiabatic[34] our model nevertheless predicts mobilities that are the same order of magnitude as experimental measurements. Letting λ_o 0.15 eV reduces electron mobilities in crystalline Alq_3 by a factor of five relative to the case where λ_o 0.

We investigated the effect of sample size on charge mobility in crystalline Alq_3: Fig. 2 compares the transient for a crystal measuring $10 \times 10 \times 10$ nm with that of the large crystal. Though it is evidently not possible to physically measure mobilities in such small volumes we find that the calculated mobilities are very similar to those of the large sample.

3.2 Disordered Alq_3

3.2.1 Photocurrent transients. Fig. 2 shows a typical photocurrent transient for disordered Alq_3 obtained from simulations of charge transport in a sample measuring $10 \times 10 \times 10$ nm. The very dispersive shape of the transient is consistent with a large distribution of hopping rates that arise from the positional and energetic disorder of the sample.[35] Fig. 4 shows the distribution of the value of the total outward hopping rate, $K_i \sum_f k_{if}$, of molecule i. Crystalline Alq_3 only has two peaks which correspond to each of the molecules in the unit cell (their inversion symmetry is lifted by the electric field). In contrast, the disordered morphologies exhibit a large spread in K_i. The effect of such broad rate distributions on charge transport is discussed further below.

3.2.2 Charge mobilities. Fig. 5 compares experimental mobilities with those predicted in disordered Alq_3. Despite the various approximations made our predicted mobilities are within an order of magnitude of experimental data at medium to large fields. Furthermore, we correctly predict that the electron mobility is over two orders of magnitude greater than the hole mobility. However, we fail to predict the correct electric field dependence.

We find that the mobility is strongly dependent on the thickness of sample considered and increases by over an order of magnitude if charges are collected halfway up the sample rather than at the top. Although the thickness dependence of the mobility in disordered Alq_3 is in contrast to crystalline Alq_3, such behaviour is expected for dispersive charge transport[36] and can be explained in terms of Fig. 6. This shows the path taken by over 2000 holes which successively reached the right electrode from the left within 1 ms. This suggests that

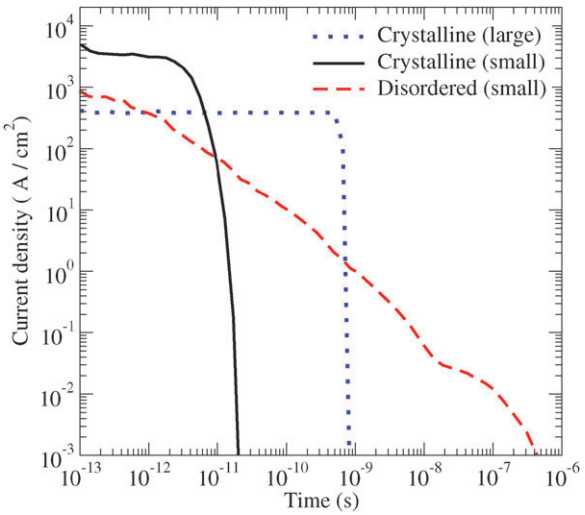

Fig. 2 Typical photocurrent transients for crystalline and disordered Alq_3 at 300 K. The large crystalline sample measures 0.03 × 0.03 × 1 μm whereas the small samples are 10 × 10 × 10 nm.

charge transport in disordered Alq_3 is dominated by a small number of molecules which collectively form highly conduct ing pathways. Indeed, on the right hand side of the sample all the holes must pass through just a handful of molecules. This mode of charge transport has been suggested before from experimental studies[37,38] and explains the thickness depen dence of the mobility: as the thickness of the film increases so does the probability that these pathways will be broken and as a result the mobility drops.

The dominance of individual pathways on charge transport and the thickness dependence of the mobility results from a large energetic disorder. Increasing the temperature reduces the effect of the energetic disorder and therefore reduces the sensitivity of the mobility to sample thickness and gives photocurrent transients that are less dispersive. In the absence

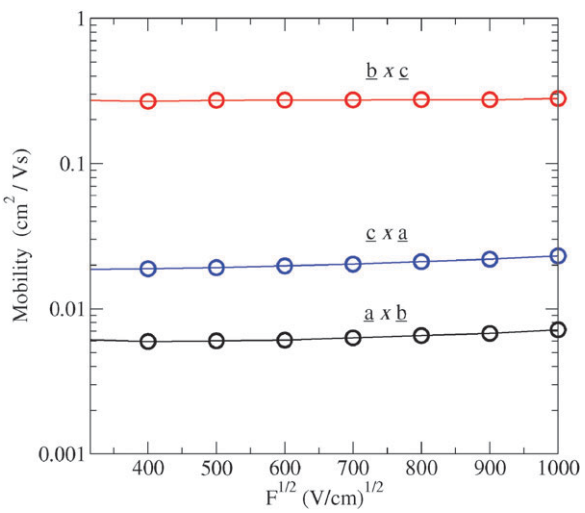

Fig. 3 Poole Frenkel plots for charge mobilities in crystalline Alq_3 at 300 K. The three lines show mobilities along electric fields that are applied perpendicular to each of the faces of the unit cell, *i.e.* $\hat{\boldsymbol{F}}$ $\hat{\boldsymbol{a}} \times \hat{\boldsymbol{b}}$; $\hat{\boldsymbol{F}}$ $\hat{\boldsymbol{b}} \times \hat{\boldsymbol{c}}$; $\hat{\boldsymbol{F}}$ $\hat{\boldsymbol{c}} \times \hat{\boldsymbol{a}}$ where $\boldsymbol{a}$, $\boldsymbol{b}$, $\boldsymbol{c}$ are the primitive lattice vectors.

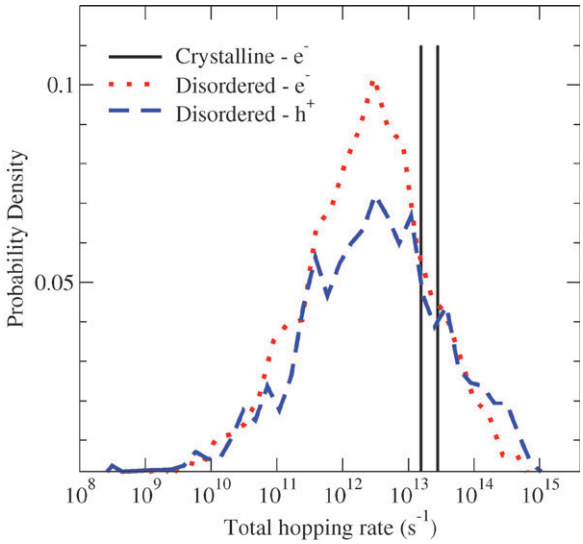

Fig. 4 Probability distribution of the total hopping rate away from a molecule K_i for electrons in crystalline Alq_3 and for both holes and electrons in disordered Alq_3 (at 300 K and 40 kV cm ^{1}).

of any energetic disorder where all $\Delta\varepsilon_{if}$ 0, almost all molecules are involved in transporting charges from one electrode to the other.

The thickness dependence of the mobility and the incorrect electric field dependence both suggest that our simulations do not accurately represent charge mobilities in bulk Alq_3. The quality of our sampling is further limited by the fact that a large fraction of molecules are not involved in charge trans port at all; disregarding the molecules on which charges are photogenerated only 25% of molecules are ever occupied at all, as shown in Fig. 6. It should also be pointed out that in our disordered sample most molecules are on the surface and therefore have fewer neighbours than would be expected in the bulk. Work is in progress to develop faster quantum

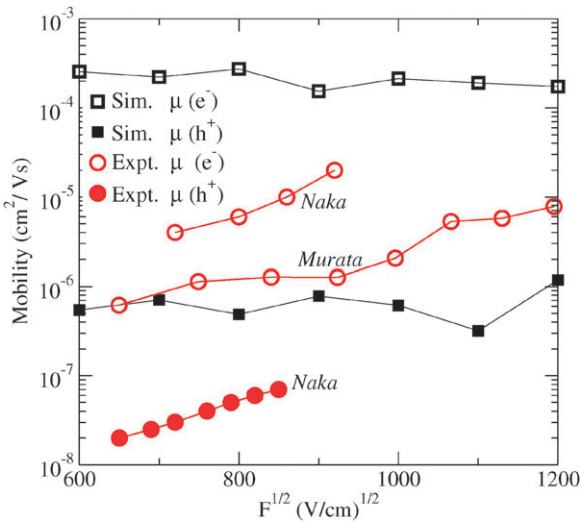

Fig. 5 Poole Frenkel plots for charge mobilities in disordered Alq_3. Simulations (squares) *vs.* experiment (circles) for electron (empty) and hole (filled) mobilities. Data from Murata *et al.*[39] (at 300 K); Naka *et al.*[14] (at 298 K).

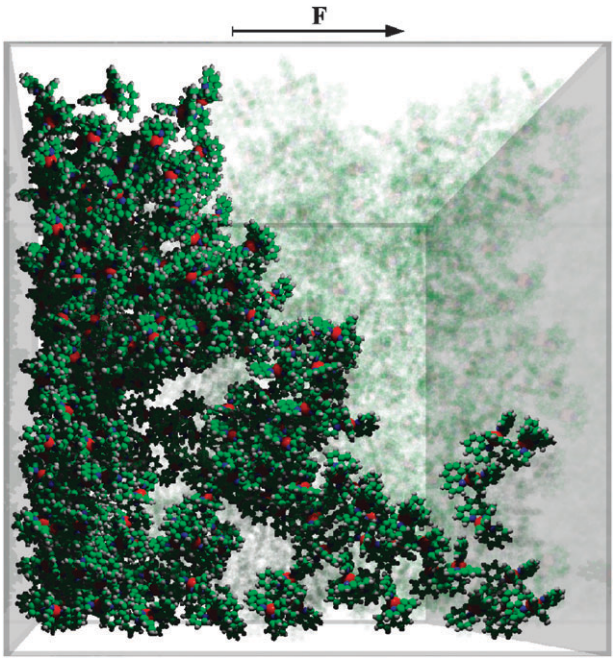

Fig. 6 Highlighted molecules are those that are occupied at least once as 2000 holes successively travel from the photogeneration region on the left to the collection region on the right.

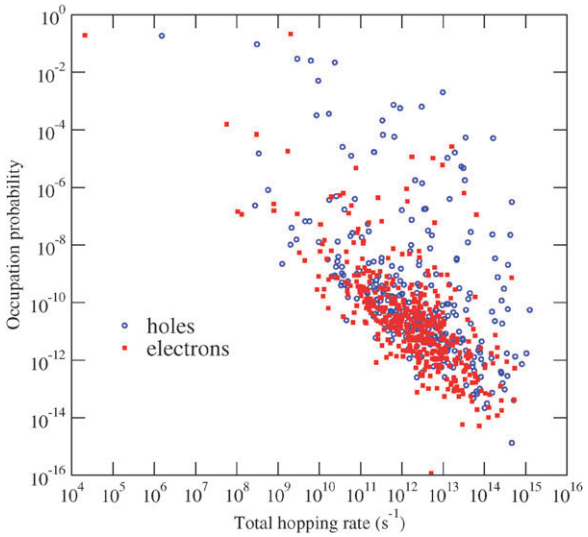

Fig. 7 Probability that a molecule is occupied (its trapping effect) against the total rate of hops away from it K_i; for hole and electron transport along the X direction.

chemical calculations that will enable simulations of larger volumes.

3.2.3 Electron *vs.* hole mobilities. It is unusual for an organic semiconductor to have mobilities that are higher for electrons than for holes. Previous theoretical studies of charge transport in Alq_3 have been limited to the crystalline phase and have concluded that hole mobilities are smaller because of weaker electronic coupling J_{if}.[15,16] However, sampling over 4000 pairs, we find that the averaged absolute electronic coupling $\langle|J_{if}|\rangle$ is greater for holes than it is for electrons, 10.2 *versus* 8.8 meV, respectively. Indeed, in the absence of energetic disorder we find that hole mobilities are two times greater than electron mobilities.

Although the average electronic coupling is greater for holes than for electrons, the energetic disorder $\langle|\Delta\varepsilon_{if}|\rangle$ is also larger (208 meV and 197 meV for holes and electrons, respectively). Moreover the distributions of J_{if} and $\Delta\varepsilon_{if}$ are both broader for holes. Therefore holes have a wider distribution of hopping rates K_i as shown by Fig. 4. Therefore one possible explanation for the lower hole mobilities is that holes are more susceptible to becoming trapped on a molecule with a small hopping rate. This is demonstrated by Fig. 7 which shows that the probability of a molecule trapping a charge is roughly inversely correlated to its total hopping rate K_i.

Though holes are more likely to be trapped by single molecules than electrons are, we find that this alone cannot account for the difference between electron and hole mobilities. Even when the 10 deepest traps are artificially removed, the hole mobility does not significantly increase. Instead we find that a second type of trapping dominates, where charges are no longer stationary on a single molecule but constantly moving amongst a small group of them. This type of trapping arises when the site energy differences are large compared to the electric field and when each molecule has a wide range of hopping rates to its neighbours. We find that holes are more often trapped in this manner and that they generally have to hop about 10 times more often than electrons before they are collected. This is consistent with the broader distribution of hole hopping rates and the greater energetic disorder that they experience. The scatter in Fig. 7 is greater for holes than it is for electrons because holes are more often trapped by a group of molecules and so the trapping effect of a single molecule depends less on its hopping rate K_i and more on its connection to other molecules.

We can rationalise the greater disorder in J_{if} and $\Delta\varepsilon_{if}$ that is experienced by holes in terms of the frontier orbitals which are shown in Fig. 8. Because the HOMO is more localised than the LUMO, the HOMO HOMO interaction between two molecules will depend more sensitively on their orientation relative to each other. This will give a greater spread in J_{if} and $\Delta\varepsilon_{if}$ for holes. In contrast, the more delocalised LUMO is expected to lead to smaller fluctuations in J_{if} and $\Delta\varepsilon_{if}$.

3.3 Conclusions

We have calculated charge mobilities in ordered and disordered Alq_3 by explicitly treating chemical structure and molecular packing. In the crystalline phase our predicted mobilities are comparable to those measured in similar organic crystals. Simulated mobilities in disordered Alq_3 are within an order of magnitude of experimental mobilities at middle to high fields though we show that dispersive transport cannot be accurately represented by such small morphologies. We suggest that charge transport in Alq_3 films is likely to be dominated by a small number of molecules which form highly conducting pathways. We correctly predict that mobilities are higher for electrons than for holes and show that, contrary to the suggestions of previous studies, this cannot be attributed simply to differences in the electronic coupling. Instead we demonstrate that some consideration of the energetic disorder

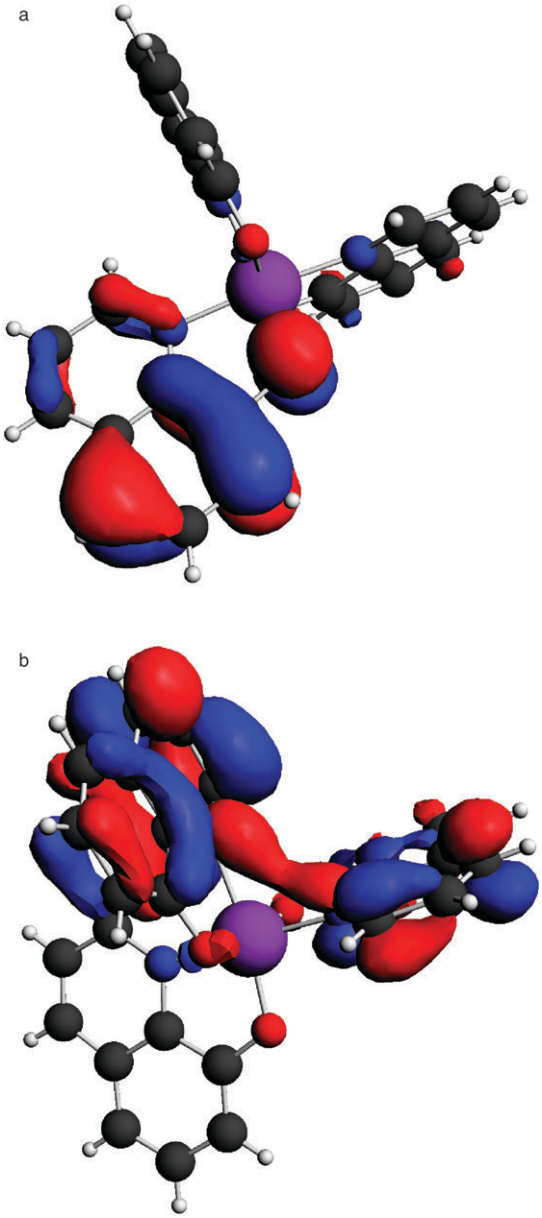

Fig. 8 The frontier orbitals of Alq_3.

is also needed. We suggest that holes experience more disorder than electrons do because the HOMO of Alq_3 is more localised than the LUMO and is therefore more susceptible to orienta tional disorder. The authors are currently developing more efficient methods that will allow more accurate calculation of the external reorganisation energy and site energies, and which will allow larger samples to be considered.

References

1 I. Mcculloch, *Nat. Mater.*, 2005, **4**(8), 583 584.
2 J. Nelson, *Curr. Opin. Solid State Mater. Sci.*, 2002, **6**(1), 87 95.
3 G. H. Gelinck, H. E. A. Huitema, E. Van Veenendaal, E. Canta tore, L. Schrijnemakers, J. B. P. H. Van der Putten, T. C. T. Geuns, M. Beenhakkers, J. B. Giesbers, B. H. Huisman, E. J. Meijer, E. M. Benito, F. J. Touwslager, A. W. Marsman, B. J. E. Van Rens and D. M. De Leeuw, *Nat. Mater.*, 2004, **3**(2), 106 110.
4 H. E. Katz, *Chem. Mater.*, 2004, **16**(23), 4748 4756.
5 C. D. Dimitrakopoulos, A. R. Brown and A. Pomp, *J. Appl. Phys.*, 1996, **80**(4), 2501 2508.
6 J. Bredas, D. Beljonne, V. Coropceanu and J. Cornil, *Chem. Rev.*, 2004, **104**(11), 4971 5003.
7 V. Coropceanu, J. Cornil, D. A. da Silva, Y. Olivier, R. Silbey and J. L. Bredas, *Chem. Rev.*, 2007, **107**(5), 2165 2165.
8 O. D. Jurchescu, J. Baas and T. T. M. Palstra, *Appl. Phys. Lett.*, 2004, **84**(16), 3061 3063.
9 R. Kline and M. McGehee, *Polym. Rev.*, 2006, **46**(1), 27 45.
10 H. Bassler, *Phys. Status Solidi B*, 1993, **175**(1), 15 56.
11 T. Kreouzis, D. Poplavskyy, S. Tuladhar, M. Campoy Quiles, J. Nelson, A. Campbell and D. Bradley, *Phys. Rev. B*, 2006, **73**(23), 235201.
12 J. Kirkpatrick, V. Marcon, J. Nelson, K. Kremer and D. Andrien ko, *Phys. Rev. Lett.*, 2007, **98**(22).
13 S. Athanasopoulos, J. Kirkpatrick, D. Martinez, J. Frost, C. Foden, A. Walker and J. Nelson, *Nano Lett.*, 2007, **7**(6), 1785 1788.
14 S. Naka, H. Okada, H. Onnagawa, Y. Yamaguchi and T. Tsutsui, *Synth. Met.*, 2000, **111**, 331 333.
15 B. Lin, C. Cheng, Z. You and C. Hsu, *J. Am. Chem. Soc.*, 2005, **127**(1), 66 67.
16 Y. Yang, H. Geng, S. Yin, Z. Shuai and J. Peng, *J. Phys. Chem. B*, 2006, **110**(7), 3180 3184.
17 E. Valeev, V. Coropceanu, D. da Silva, S. Salman and J. Bredas, *J. Am. Chem. Soc.*, 2006, **128**(30), 9882 9886.
18 A. Troisi, *Mol. Simul.*, 2006, **32**(9), 707 716.
19 K. Freed and J. Jortner, *J. Chem. Phys.*, 1970, **52**(12), 6272.
20 M. Brinkmann, G. Gadret, M. Muccini, C. Taliani, N. Masciocchi and A. Sironi, *J. Am. Chem. Soc.*, 2000, **122**(21), 5147 5157.
21 M. Colle, J. Gmeiner, W. Milius, H. Hillebrecht and W. Brutting, *Adv. Funct. Mater.*, 2003, **13**(2), 108 112.
22 A. Verma, A. Schug, K. Lee and W. Wenzel, *J. Chem. Phys.*, 2006, **124**(4).
23 D. Wales and J. Doye, *J. Phys. Chem. A*, 1997, **101**(28), 5111 5116.
24 T. Bogdan, D. J. Wales and F. Calvo, *J. Chem. Phys.*, 2006, **124**, 044102.
25 S. Kirkpatrick, C. Gelatt and M. Vecchi, *Science*, 1983, **220**(4598), 671 680.
26 S. L. Mayo, B. D. Olafson and W. A. Goddard, *J. Phys. Chem.*, 1990, **94**(26), 8897 8909.
27 H. Li, J. L. Bredas and C. Lennartz, *J. Chem. Phys.*, 2007, **126**(16).
28 J. Perdew, J. Chevary, S. Vosko, K. Jackson, M. Perderson, D. Singh and C. Fiolhais, *Phys. Rev. B*, 1992, **46**(11), 6671 6687.
29 G. Velde, F. Bickelhaupt, E. Baerends, C. Guerra, S. Van Gisber gen, J. Snijders and T. Ziegler, *J. Comput. Chem.*, 2001, **22**(9), 931 967.
30 I. Vilfan, *Phys. Status Solidi B*, 1973, **59**(1), 351 360.
31 A. Chatten, S. Tuladhar, S. Choulis, D. Bradley and J. Nelson, *J. Mater. Sci.*, 2005, **40**(6), 1393 1398.
32 W. Warta, R. Stehle and N. Karl, *Appl. Phys. A*, 1985, **36**(3), 163 170.
33 J. Y. Lee, S. Roth and Y. W. Park, *Appl. Phys. Lett.*, 2006, **88**(25).
34 A. Troisi and G. Orlandi, *Phys. Rev. Lett.*, 2006, **96**(8).
35 H. Scher and E. Montroll, *Phys. Rev. B*, 1975, **12**(6), 2455 2477.
36 H. Scher, M. Shlesinger and J. Bendler, *Phys. Today*, 1991, **44**(1), 26 34.
37 M. Colle, M. Buchel and D. de Leeuw, *Org. Electron.*, 2006, **7**(5), 305 312.
38 G. Matt, N. Sariciftci and T. Fromherz, *Appl. Phys. Lett.*, 2004, **84**(9), 1570 1572.
39 H. Murata, G. Malliaras, M. Uchida, Y. Shen and Z. Kafafi, *Chem. Phys. Lett.*, 2001, **339**(3 4), 161 166.